2015 IEEE/RSJ International Conference on Intelligent Robots and Systems (IROS)
Congress Center Hamburg
Sept 28 - Oct 2, 2015. Hamburg, Germany

A 7.5mm Steiner chain fibre-optic system for multi-segment flex sensing

S. Sareh, Y. Noh, T. Ranzani, H. Wurdemann, H. Liu, K. Althoefer, *Member, IEEE*

***Abstract*— This paper presents a highly compact fibre-optic system based on light intensity modulation for multi-segment flex sensing in pliable robot arms, e.g., articulated surgical instruments. This fibre-optic arrangement is 7.5 mm in diameter and is comprised of a two-segment flexible and stretchable Steiner chain arm section with twelve housings at the distal side which accommodates passive cables. The displacement of each cable will be used to determine the bending. This Steiner chain section is followed by a basal rigid fibre-optic sensing unit integrated with a low-friction retractable distance modulation array which couples the motion of the passive cables with light-emitting optical fibres. The low-friction retractable distance modulation array uses steel spring-needle double sliders to reduce the hysteresis and to recover reference sensor values when the arm returns to its original straight configuration. The U-shape loopback design of the optical fibres allows integration of all electronics away from the sensing site. The experimental results indicate a maximum bending angle error of 6º in one individual segment of the two-segment arm with respect to reference angle values calculated from camera images.**

I. Introduction

Sensing technologies suitable for integrating into the new highly redundant [1] [2] and soft [3] [4] class of robotic arms [5-8] are becoming increasingly demanded due to the inclusive nature of these manipulation systems enabling medical [9-11] and robotic [12] [13] applications in confined space. These robotic systems are usually made from mutually-tangent curved segments enabling high degrees of robotic articulation in unstructured and cluttered workspaces [4] [10] [15] [26]. The piecewise bendable and extensible segments enable bending around objects and reaching targets which are inaccessible by conventional rigid robotic arms. However, position control of these robotic systems requires precise shape sensing which is achievable through multi-segment flex sensing.

The complex motion patterns generated by flexible robots have been mainly tracked through incorporation of vision systems [16] and electromagnetic tracking [17], especially when used in medical applications. However, the visual tracking is often restricted due to visual occlusions and electromagnetic tracking is subject to magnetic field distortions and have limitations with regards to mobility of the magnetic field generation system.

The work described in this paper is funded by the Seventh Framework Programme of the European Commission under grant agreement 287728 in the framework of EU project STIFF-FLOP.

S. Sareh, Y. Noh, H. Wurdemann, H. Liu, and K. Althoefer are with Centre for Robotics Research, King's College London, UK.

Tommaso Ranzani is with the Harvard John A. Paulson School of Engineering and Applied Sciences, Wyss Institute for Biologically Inspired Engineering, Harvard University, Cambridge, MA, USA.

There are various ways of sensing flexion through passive resistive devices made from conductive inks and fabrics, e.g., the Flexpoint sensor (Flexpoint Sensor Systems, Inc, USA), and specific types of bipolar smart materials, e.g., Ionic Polymer Metal Composites (IPMCs) [18]. However, these techniques are usually not suitable for three dimensional sensing. Fiber Bragg Grating (FBG) shape sensing tubes were proposed for shape sensing in continuum robots in [19]. The FBG sensors are highly sensitive to the change of environmental temperature and strain. In the case of a non-uniform strain field, the strain compensation is challenging [20]. Shape sensing based on FBG is not suitable for extensible systems. Light intensity modulation [7] [21] [22] is another optical approach that can be adapted for flex sensing [23] [24]. This approach is temperature independent [23] and low-cost.

In this paper, we present the design and creation of an extensible multi-segment flex sensor based on light intensity modulation between two optical fibre tips.

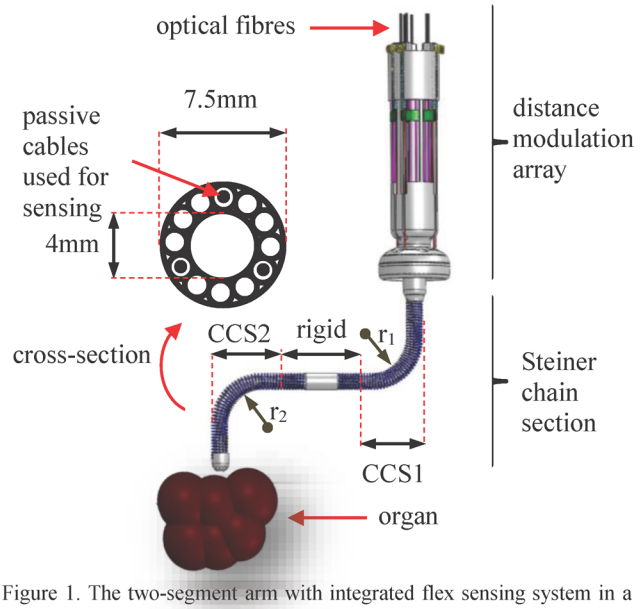

Figure 1. The two-segment arm with integrated flex sensing system in a surgical scenario interacting with an organ. Note that the flexible section also provides an empty central channel for end-effector instruments (CCS1 and CCS2 indicate constant curvature segments with radii of r_1 and r_2, respectively).

II. Design of the Flex Sensing System

The flex sensing system comprised of a Steiner chain flexible arm section responsible for maintaining the radial distance between the passive cables used for sensing and the centre of the flexible arm during manipulations at the distal side and a distance modulation array which couples the motion of passive cables with light-emitting optical fibres

using a low-friction sliding mechanism at the proximal side. Each light emitting optical fibre is paired and aligned with an optical detector fixed at the base.

The flexible arm shown in Fig. 1 has two flexible segments each 30mm long. The flex sensing system uses three tiny spring channels (1.2 mm outer diameter) equally spaced around the central axis of the arm with a radius *d*. The spring channels are accordingly extended outside the arm into a rigid 3D printed part with sliding rails and plates. There are two passive cables fed through each channel; the shorter cable is fixed between the tip of the base segment and a sliding plate; the longer cable is fixed between the tip of the tip segment and a sliding plate. Therefore the sensing system uses six sliding plates in total. Each plate is sliding using a low friction steel-needle mechanism and is attached to the base using a 2 mm outer diameter extension spring to recover the position of the sliding plates after being pulled by driving cables. The sliding plates employ a υ-shaped structure to be able to house light emitting optical fibres. A U-shape light-emitting optical fibre is integrated inside each plate and aligned with a light detector fixed at the base. Therefore each sliding plate is the interface between a passive cable of the Steiner chain section and an optical fibre of the distance modulation array, so we shall call it a υ-shaped mechano-optical coupler in this paper. These couplers are designed and fabricated to be able to smoothly slide around needles and carry the light-transmitting optical fibres inside the sensor base. This arrangement allows the flex sensor to exploit a retractable sliding mechanism for modulating the distance *h* between emitter and detector optical fibres (Fig. 3b). This distance is measured using a FS-N11MN fibre optic sensor (Keyence™, Japan), in this study.

A. The Steiner chain section

In geometry, a Steiner chain is a closed set of mutually-tangent *n* circles, all of which are also tangent to two given non-intersecting circles, just like the structure illustrated in Fig. 2a. The Steiner chain mathematics can represent the design of a steerable endoscope in [25], where low-cost commercial springs are tangentially combined in parallel to tightly accommodate driving cables and prevent their radial displacement. Fig. 2a also illustrates the cross section of such actuation mechanism. Clearly, this structure can also house passive cables to code the shape of the endoscope or similar manipulation systems. In this paper, we incorporate this analogy and create a more systematic design approach.

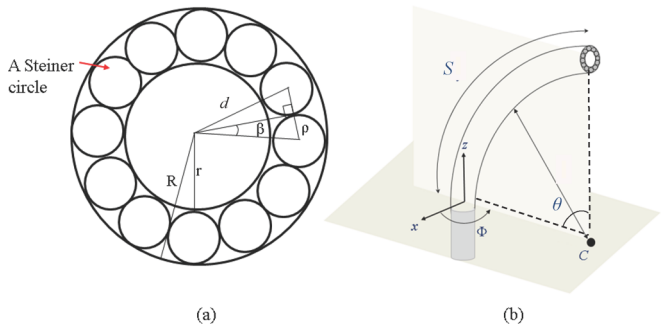

Figure 2. (a) The Steiner chain cross-section of the arm and (b) the flexed configuration of the arm and associated parameters in 3D [26].

The flex sensor of each segment of the arm consists of three passive cables sliding inside flexible Steiner chain housings in the periphery of the arm in parallel with driving cables as illustrated in Fig. 1. When the arm bends, the cables' length portion inside the flexible arm (s_1, s_2, and s_3) will change according to the pose of the arm. Note that the displacement of any passive cable h_i (indicated in Fig. 3a), i is the cable number, causes a change in the position of the light emitting optical fibres and, consequently, the intensity of the light received by light detectors, e.g., FS-N11MN. Therefore the displacement h_i should be measured and added to the passive length of the arm (L=30mm) to result the length of cables which are fed inside the flexible arm. The received light by FS-N11MN is, hence, measured and converted into voltage $v = [v_1\ v_2\ v_3]$ and related to the corresponding distance vector $s = f(v) = [s_1\ s_2\ s_3]$ to acquire configuration parameters of arm segment for each specific pose. The configuration parameters consist of: S is the length of the central axis of the each segment, θ is the bending angle, and φ is the orientation angle (see Fig. 2b and Equations (1)-(3)) [26].

$$S = \frac{1}{3}\sum_{i=1}^{3}(s_i) \tag{1}$$

$$\theta = \frac{S - s_1}{d.\cos(\frac{\pi}{2} - \varphi)} \tag{2}$$

$$\varphi = \tan^{-1}\left(\frac{\sqrt{3}(s_2 + s_3 - 2s_1)}{3(s_2 - s_3)}\right), \tag{3}$$

where the variable d in Equation (2) describes the distance between the central axis of the arm segment and the parallel passive cables. In the following, we show that any change in s_1, s_2, and s_3 cause by bending is affected by the radius d. Therefore, changing d result in changing the resolution of the sensory system.

By substituting $\varphi_1 = \frac{\pi}{2}$ and a very small amount of bending $\theta_1 = \frac{\pi}{180}$ in Equations (3) and then (2), it yields

$$-2s_{1,1} + s_{2,1} + s_{3,1} = 0.0525d, \tag{4}$$

where $s_{i,1}$ denotes the primary length of the cable i which is inside the arm segment. Also from Equation (3), $s_{2,1} = s_{3,1}$. Therefore, it yields

$$s_{2,1} - s_{1,1} = 0.0262d\,. \tag{5}$$

If substituting $\varphi_2 = \frac{\pi}{2}$ and $\theta_2 = \frac{\pi}{2}$ in the same set of equations

$$s_{2,2} - s_{1,2} = \frac{3\pi}{4}d, \tag{6}$$

where $s_{i,2}$ explains the secondary length of the cable i which is inside the arm segment. The total change in the length of the cable s_1 can be obtained by subtracting Equations (5) and (6):

$$\Delta s_1 = s_{2,2} - s_{1,2} - s_{2,1} + s_{1,1}. \tag{7}$$

The arm segments are made from extension springs and are, therefore, incompressible. Assuming $s_{2,2} \approx s_{2,1}$, the

change in the cable's length inside the arm can be calculated by

$$\Delta s_1 \approx \frac{3\pi}{4} d. \quad (8)$$

The FS-N11MN fibre optic sensor used in this study can effectively measure the light intensity when the distance between light-emitting and light detecting optical fiber tips is less than 20 mm. In order to measure a 90° bending deformation, the maximum value of d must not exceed 8.4 mm. It is clear that, this value should be reduced to 4.2mm for measuring a maximum of 180° bending which can be regarded as two successive 90° bending as targeted in this study. Since the maximum combined deformation of the two segments should be also measureable within this 20 mm range, d_{max} needs to be 2.1mm.

To preserve the maximum resolution of the sensing system, we opt for the maximum value for d, which is 2.1 mm. This necessitates incorporating an inner spring with a diameter of slightly less than 4mm. We have, therefore used LEM050AB 05 S stainless steel extension spring (Lee Spring Ltd., USA) with an outer diameter of 3.505 mm and a wire diameter of 0.508 as the central spine. For Steiner springs (corresponding to a Steiner circle in the cross-section view, see Fig. 2a), we have used custom springs with an outer diameter of 1.2 mm and a wire diameter of 0.25 mm. Steel passive cables used for sensing with a diameter of 0.27 mm (Carl Stahl Ltd., Germany) are radially fixed at approximately d=2.1mm away from the centre. The central angle $\beta=\sin^{-1}\left(\frac{\rho}{r+\rho}\right)$ can be calculated as approximately 15°. The number of Steiner springs is $n=\frac{180}{\beta}=12$ and the inner diameter of the outer spring should be approximately R= r+2 ρ=5.91mm. We have selected LEM070CB 05 S (Lee Spring Ltd., USA) with an outer diameter of 7.49 mm and a wire diameter of 0.711 mm.

The arm section of the sensing system is comprised of twelve Steiner channels. The design uses three of them for sensing; these channels pass through the whole length of the two segment arm and house passive cables. The design also considers six channels for housing driving cables. Therefore, three channels are empty and can be used for other applications, e.g. end-effector tool's wiring.

B. *Design of a low-friction retractable distance modulation array*

In response to a bending deformation, the portion of length of each passive cable, which is inside the arm, will change. When the arm returns to its original straight configuration, cables' length portion inside the arm are also required to follow back to the original. Several reasons including friction, and hysteresis in the mechanical structure and material properties prevent fulfilling this essential condition and introduce malfunction into the sensory system. In order to make sure the mutual distance between the emitting and detecting fibre optic pairs is recovered, a spring returning mechanism is a very natural solution. In addition, this mechanism couples the motion of passive cables that are passed through the length of the flexible arm with optical fibres for distance measurement using FS-N11MN sensors.

1) *Loopback design of the optical system*

The commercial off-the-shelf stretch (length) sensors e.g. stretch sensors from StretchSense Ltd, New Zealand, and PolyPower® Stretch Sensors, are usually fabricated to be free from electronics at one end. This free end is usually coupled with the moving end of the actuator to measure the length change. Here, in order to allow all the electronics to be at one end of the sensor we employed a U-shape arrangement of optical fibres to produce a loopback configuration. This enables placing the emitter and detector next to each other, as illustrated in Fig. 3(b).

2) *The Steel spring-needle double slider*

A low-friction sliding mechanism is also essential to enable modulating the mutual distance between any pair of optical fibres. In order to address this requirement, we have fabricated a highly smooth double slider using two steel needles (44mm length x 0.86mm diameter, John James Needles, Worcestershire, England), surrounded by two small-sized pieces of steel springs (1.4 mm outer diameter, 0.2 mm wire diameter), that are anchored in parallel and 4mm away from each other into the plastic sensor base. Each steel spring that is able to smoothly slide around the surrounded needle, is embedded into a ʊ-shaped plastic mechano-optical coupler. Each coupler links a passive cable with its corresponding fiber optic pair. This mechanism is shown in Fig. 3(d). Fig. 3(c) illustrates the cross-section of the distance modulation array with its maximum outer diameter of 22 mm.

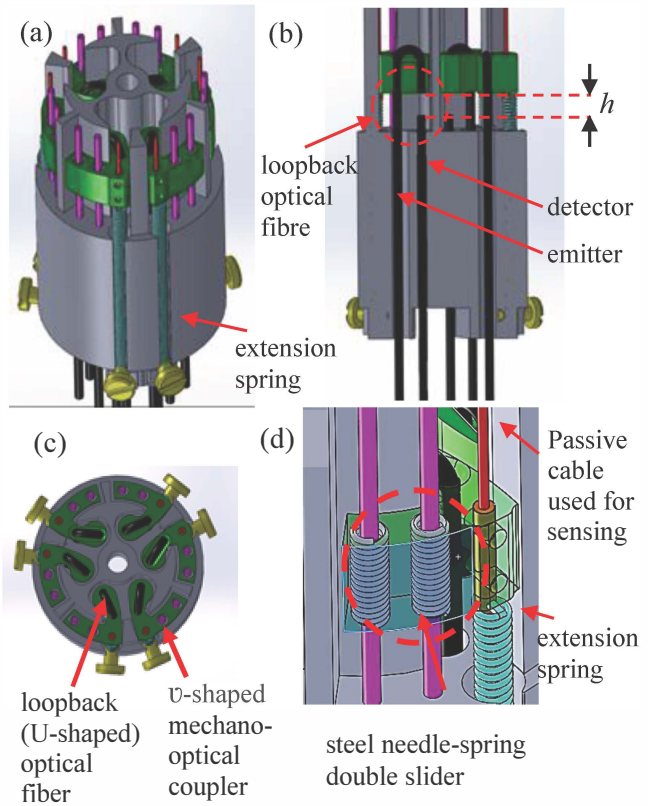

Figure 3. The CAD designs of the multi-segment flex sensor exhibiting integrated technologies: (a) the side view of the distance modulation array showing the elastic recovery mechanism of the slider, (b) the U-shape loopback fibre optic arrangement for keeping electronics away from the sensing site, (c) the cross-section of the distance modulation array, and (d) the low-friction steel spring-needle double sliding mechanism to maintain the direction of the motion.

III. FABRICATION AND ASSEMBLY

The sensorised arm in its finished configuration is shown in Figs. 4(a) and 4(b). The disassembled structure of the mechano-optical coupler is demonstrated in Fig. 4(c), comprising of a υ-shaped 3D printed plate part with an U-shaped housing for an optical fibre, and a connection module which links a 2 mm outer diameter extension spring (Lee Spring Ltd., USA), with a 0.27 mm thick steel passive cable (Carl Stahl, Germany). Note that these 2 mm extension springs are responsible for cables position recovery and therefore we call them recovery springs. We have considered an initial stretch of 5 mm in recovery springs to increase the pulling force. Finally, Figs 4(d) and 4(e) present the fully assembled structure of the main top (Steiner chain), and the bottom (distance modulation array) parts of the arm. All plastic parts were fabricated using a rapid prototyping machine (Project HD-3000 Plus, 3D Systems).

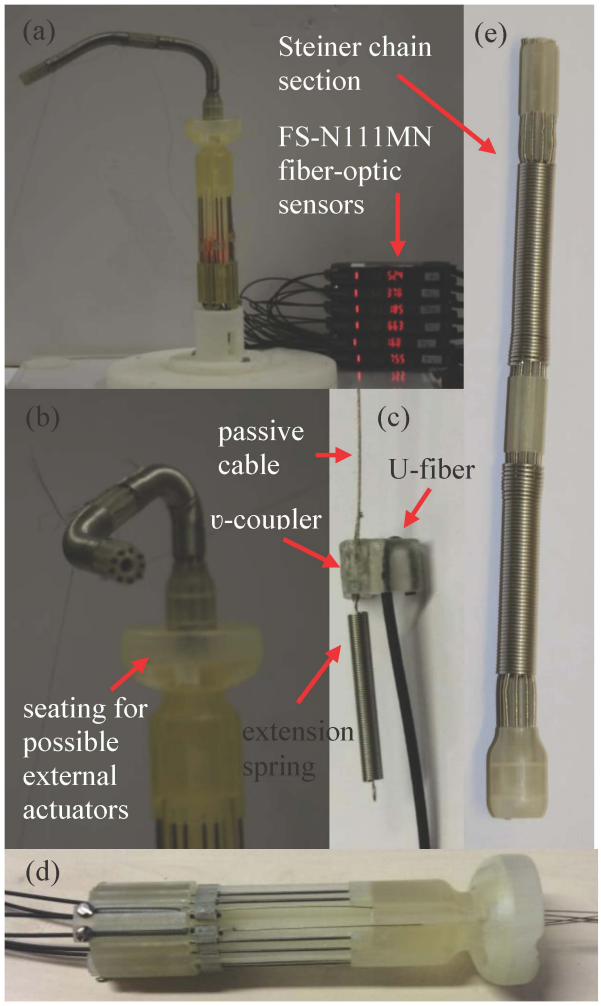

Figure 4. The prototype of the arm and sensing system: (a) the finished configuration of the sensorised manipulation system, (b) close-up view of the top part, (c) the υ-shaped mechano-optical coupler, (d) the fully assembled structure of the distance modulation array, and (e) the structure of the Steiner chain section.

IV. EXPERIMENTAL CALIBRATION AND FLEX SENSING VALIDATION

In order to validate the design and implementation of the two-segment flex sensor, we have performed a set of experiments where either one or both segments were actuated at time. Two HD cameras were placed at the top and side of the manipulator to record ground truth flex information. The present manipulation platform is not yet equipped with motors or other actuators. So we attached the middle and tip of the arm to fixed points on the wall, using steel wires, in order to generate stable shape patterns. Subsequently we have recorded the light intensity (and corresponding voltage) values from FS-N11MN fibre-optic sensors and cameras.

To convert voltage values to corresponding values of distance between optical fibre tips h, we have extracted the calibration relationship for all six fibre optic channels. The averaged calibration data, presented together with error bars in Fig. 5, was splined in MATLAB (MathWorks, Inc., Natick, MA) to form the calibration curve.

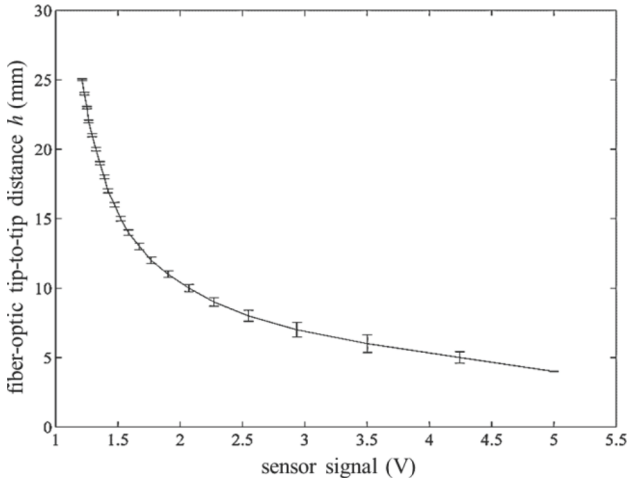

Figure 5. The averaged calibration curve and error bars

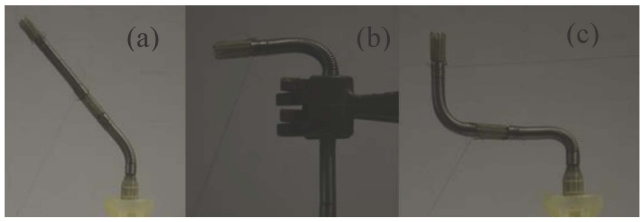

Figure 6. Examples of key experimental configurations: (a) independent activation of base segment, (b) independent activation of the tip segment (note that the intersegment link is clamed to produce a stationary base), and (c) simultaneous activation of two segments.

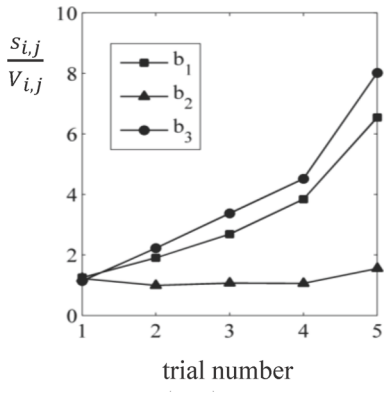

Figure 7. The $s_{i,j}/V_{i,j}$ values for the base segment experiment.

Having calibrated the sensors, the manipulator was forced into various three dimensional shapes, shown in Figure 6 and the sensor signals were recorded and analyzed.

In order to use the constant curvature bending model, the acquired voltage signals were fed into the splined calibration data presented in Fig. 5 to back-calculate the tip-to-tip fibre optic distances. Subsequently, these distances were substituted into equations (2) and (3) to calculate the bending curvature of the manipulator. Fig. 8 shows the experimental results compared with their corresponding ground truth information extracted from camera images using a custom MATLAB (MathWorks, Inc., Natick, MA) code.

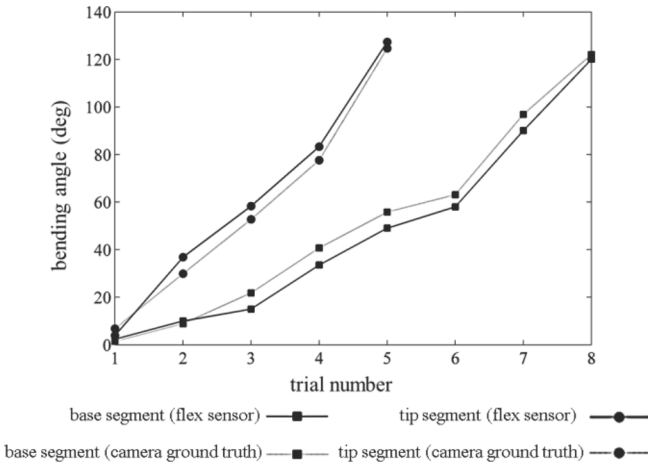

Figure 8. The experimental results of flex sensing in individual segments.

In Fig. 7, $s_{i,j}$ represents the tip-to-tip distance between optical fibre pair, where i={1,2,3} is the pair number and j ={1,2,3,4,5} is the trial number. The trend in $s_{i,j}/V_{i,j}$ implies that the arm was flexed approximately symmetric with respect to cables b_1 and b_3, where these two cables are virtually stretched (physically only the length portion of cables inside the arm can change). The cable b_2 was only slightly compressed, with respect to the length change in other two cables which confirms the design assumption led to Equation (8).

Fig. 8 shows the experimental results, where segments of the arm were actuated individually, implying a maximum tracking error of around 7° in tip segment when the arm was flexed with ground truth value of 40°. This error was decreased to 5° as the arm reached a ground truth bending angle of 63° and around 2° for ground truth value of 122°. A similar behaviour can be seen in the flex data, also presented in Fig. 8, of the base segment. The finer behaviour of the sensor for large flexions can be due to better positioning of cables inside the spring channels. These channels have an internal diameter of around 0.8mm and are housing two 0.27 mm thick cables, along the length of the base segment and only one of them along the length of the tip segment. So there is some room for cables to play radially, if they are not pulled tightly using extension springs. However, we have considered a pre-stretch of 5mm in the design, the experimental results implies that the error can be reduced if this initial stretch is increased.

V. Calculation of the Bending Curvature in a Two-Segment Arm Based on Collocated Cables

In order to simplify the multi-segment curvature sensing, this work exploits a method which we call "collocated cables". As mentioned in section II.A this sensing arrangement uses only three Steiner channels out of twelve for sensing. There are two passive cables sliding inside each of these three channels; one fixed between two segments and the other one at the tip of the arm. This allows measuring the bending angle in multi-segment arms in a modular way, in the sense that the Steiner chain structure remains the same for all segments. When the arm undergoes a complex two-segment movement, the change in the length of cables passing through the whole length of the arm to the tip (t-type cables t_1, t_2, and t_3), is only partially due to the bending of the tip segment. However, the change in the length of the fibres fixed at the tip of the base segment (b-type cables b_1, b_2, and b_3) is purely due to the bending in this segment. In our sensing arrangement, each t-type cable is companied by a b-type cable, as shown in Fig. 9. This allows calculating the share of each segment from the total length change.

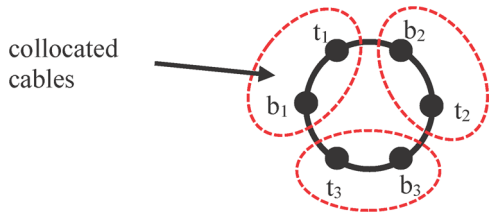

Figure 9. The cross-section of the distance modulation array, showing the collocated arrangement of passive cables used for sensing.

To intuitively evaluate this method, we moved segments of the arm into a complex S-shape configuration, shown in Fig. 6(c). Using camera ground truth information, we have calculated the bending angle in two segments as $\theta_{Ground,1}$=91.2°, $\theta_{Ground,2}$=95.1°.

TABLE 1 summarizes the calculation of length change in each segment based on collocated cables' lengths; V_{bi} values, i={1,2,3}, represent FS-N11MN voltage readings associated with cables that are fixed between two segments; V_{ti} are readings associated with cables passed through the whole length of the arm and fixed at the tip. Mapping into the splined voltage-distance relationship, Fig. 5, corresponding fibres' mutual displacements s_{bi} and s_{ti} are calculated. Whilst values of s_{bi} are representing the pure cable's length change in the base segment, the pure length change of cables in the tip segment can be computed through $s_{pi}=s_{ti}-s_{bi}$.

TABLE 1. CALCULATION OF THE PURE LENGTH CHANGE IN EACH SEGMENT BASED ON COLLOCATED CABLES APPROACH.

Voltage (V)	V_{b1}	V_{b2}	V_{b3}	V_{t1}	V_{t2}	V_{t3}
	3.99	2.92	1.93	1.89	2.27	1.93
Length (mm)	s_{b1}	s_{b2}	s_{b3}	s_{t1}	s_{t2}	s_{t3}
	5.34	7.04	10.87	11.11	9.01	10.87
Length (mm)	s_{p1}		s_{p2}		s_{p3}	
	5.77		1.96		0	

By substituting pure displacement values into equations (1) to (3), the sensory bending angles are computed as $\theta_{Sensor,1}$=89.2° and $\theta_{Sensor,2}$=92.4°. This implies an error of less than 3° in each segment.

VI. CONCLUSIONS AND FUTURE WORKS

In this paper, we have presented the design and fabrication of a flex sensing system for a 7.5mm multi-segment flexible manipulation arm. Starting from theoretical design, we have optimised the radial location of the passive cables used for sensing along the periphery of the arm in order to represent a trade-off between maximum compactness of the sensing system and using the full capacity of the optical measurement system in terms of the measurement resolution. In the next step, we have presented a Steiner chain design (n=12) for the flexible part of the sensor system. Three out of twelve Steiner chain channels were used for flex sensing in the two-segment flexible arm. Subsequently we have designed and fabricated a low-friction fibre-optic distance modulation array based on a new spring-needle double slider to precisely measure the change in the length of cables which are fed inside the flexible arm during bending. The design also employs a loopback optical method to keep all electronics away from of the sensing site. Finally, the complete sensing system is implemented and experimentally evaluated, resulting in a maximum error of 6° with respect to the used camera ground truth information in measuring the bending angle in one individual segments. From the experimental results, it can be implied that the sensing error can be decreased by increasing the initial stretch length of recovery springs, to have a tighter cable system in low bending angles. We have also demonstrated the multi segment flex sensing exploiting collocation of passive cables in successive segments. This sensing system can be regarded as complimentary for the two-segment soft actuation system presented in [9] [10].

Future work will focus on further development of the flexible arm, by activating its internal actuation mechanism using driving cables and motors. Having installed actuators, we will have the opportunity to produce various motion patterns and characterise the entire sensing workspace.

ACKNOWLEDGMENT

The work described in this paper is funded by the Seventh Framework Programme of the European Commission under grant agreement 287728 in the framework of EU project STIFF-FLOP.

REFERENCES

[1] H. Yamada, S. Chigisaki, M. Mori, K. Takita, K. Ogami, S. Hirose, "Development of amphibious snake-like robot ACM-R5". Proc. 36th Int'l Symp. Robotics 36, 133, 2005.

[2] K. Lipkin, I. Brown, A. Peck, H. Choset, J. Rembisz, P. Gianfortoni, A. Naaktgeboren. "Differentiable and piecewise differentiable gaits for snake robots". In Proc. IEEE Int'l Conference on Intelligent Robots and Systems, 1864 – 1869. San Diego, CA, 2007.

[3] M. Calisti, M. Giorelli, G. Levy, B. Mazzolai, B. Hochner, C. Laschi, P. Dario "An octopus-bioinspired solution to movement and manipulation for soft robots". Bioinspir Biomim. 6(3):036002, 2011.

[4] D. Trivedi, C. Rahn, W. Kier, I. Walker. "Soft robotics: biological inspiration, state of the art, and future research". Appl. Bionics. Biomech. 5, 99 – 117, 2008.

[5] Vogt, D.M.; Yong-Lae Park; Wood, R.J., "Design and Characterization of a Soft Multi-Axis Force Sensor Using Embedded Microfluidic Channels," *Sensors Journal, IEEE* , vol.13, no.10, pp.4056,4064, Oct. 2013.

[6] Y., Noh, S., Sareh, J., Back, H., Würdemann, T., Ranzani, E.L., Secco, A., Faragasso, H., Liu, K. Althoefer (2014) Development of a Three Axial Body Force Sensor for Flexible Manipulators, IEEE Int'l Conference on Robotics and Automation (ICRA) 2014.

[7] S. Sareh, A. Jiang, A. Faragasso, Y. Noh, T. Nanayakkara, P. Dasgupta, L.D. Seneviratne, H.A. Wurdemann, K. Althoefer, "Bio-Inspired Tactile Sensor Sleeve for Surgical Soft Manipulators", IEEE Int'l Conference on Robotics and Automation (ICRA 2014), Hong Kong, 2014.

[8] Y. Noh, E.L. Secco, S. Sareh, H.A. Wurdemann, H. Liu, K. Althoefer "A Continuum Body Force Sensor Designed for Flexible Surgical Robotic Devices" IEEE Engineering in Medicine and Biology Society, 2014.

[9] M. Cianchetti, T. Ranzani, G. Gerboni, I. De Falco, C. Laschi, A. Menciassi "STIFF-FLOP Surgical Manipulator: mechanical design and experimental characterization of the single module", IEEE/RSJ Int'l Conference on Intelligent Robots and Systems (IROS), 2013.

[10] T. Ranzani, G.Gerboni, M. Cianchetti, A.Menciassi. " A bioinspired soft manipulator for minimally invasive surgery", IOP *Bioinspir. Biomim.* 10 035008, Special issue on octopus inspired robots, 2015.

[11] J. Shang, D. Noonan, C. Payne, J. Clark, M. H. Sodergren, A. Darzi, G.-Z. Yang, "An Articulated Universal Joint Based Flexible Access Robot for Minimally Invasive Surgery", IEEE Int'l Conference on Robotics and Automation. pp. 1147-1152, 2011.

[12] A. Degani, H. Choset, B. Zubiate, T. Ota and M. Zenati, "Highly Articulated Robotic Probe for Minimally Invasive Surgery, " in 30th Annual Int'l IEEE EMBS Conference, Canada, August 2008.

[13] OC Robotics, Snake-arm robots access the inaccessible", OC Robotics, Nuclear Technology International, 2008, p92-94.

[14] S. Sareh, J.M. Rossiter, A.T. Conn, K. Drescher, R.E. Goldstein "Swimming like algae: biomimetic soft artificial cilia", *Journal of the Royal Society Interface* 20120666, 2013.

[15] S. Sareh, A.T. Conn and J. M. Rossiter, "Optimization of bio-inspired multi-segment IPMC cilia" EAPAD XII: Proc. Electroactive Polymer Actuators and Devices vol 7642 SPIE, 2010.

[16] J.M D.C. Rucker, J.M. Romano, R.J. Webster. "Visual sensing of continuum robot shape using self-organizing maps", IEEE Int'l Conference on Robotics and Automation, 4591 – 4596, 2010

[17] M. Mahvash, and D.E. Dupont, "Stiffness Control of a Continuum Manipulator in Contact with a Soft Environment", IEEE/RSJ Int'l Conference on Intelligent Robots and Systems 2010:863-870, 2010.

[18] A. Punning, M. Kruusmaa, & A. Abaloo, "Surface resistance experiments with IPMC". Sensors and Actuators A, 133(1), pp. 200-209, 2007.

[19] S. Ryu, P. E. Dupont, "FBG-based Shape Sensing Tubes for Continuum Robots", IEEE Int'l Conference on Robotics and Automation, pp. 3531-3537, 2014.

[20] X. Zhang, J.J. Max, X. Jiang, L. Yu, H. Kassi, "Experimental investigation on optical spectral deformation of embedded FBG sensors", Proc. SPIE 6478, Photonics Packaging, Integration, and Interconnects VII, 647808, 2007.

[21] P. Polygerinos, L. D. Seneviratne, and K. Althoefer, "Modeling of Light Intensity-Modulated Fiber-Optic Displacement Sensors," Actions on Instrunentation and Mesurement, vol. 60, no. 4, pp. 1408-1415, 2011.

[22] P. Puangmali, H. Liu, L. D. Seneviratne, P. Dasgupta, K. Althoefer. "Miniature 3-axis distal force sensor for minimally invasive surgical palpation". Mechatronics, IEEE/ASME Transactions on, 17(4), pp: 646-656. 2012.

[23] T.C. Searle, K. Althoefer, L.D. Seneviratne, H. Liu, "An optical curvature sensor for flexible manipulators". ICRA 2013: 4415-4420, 2013.

[24] S., Sareh, Y., Noh, T., Ranzani, H., Würdemann, H., Liu, K. Althoefer "Modular fibre-optic shape sensor for articulated surgical instruments", Hamlyn Symposium on Medical Robotics, 2015.

[25] P. Breedveld, J. Scheltes, E. Blom, and J. Verheij, "A New, Easily Miniaturized Steerable Endoscope," IEEE Eng. Med. Biol. Mag., pp. 40–47. 26, 2005.

[26] R. J. Webster III, and B. A. Jones, "Design and Kinematic Modeling of Constant Curvature Continuum Robots: A Review," International Journal of Robotics Research, vol. 29, no. 13, pp. 1661-1683, 2010.